



## RESEARCH ARTICLE

## Application of Nanosized Mesoporous Aluminosilicates for Adsorption of $Hg^{+2}$ from Aqueous Solutions: Kinetic, Isotherm and Thermodynamic Studies.

Mohamed M. Eldefrawy, Ibrahim M. M. Kenawy, Rania M. El -Tabey  
Chemistry Department, Faculty of Science, Mansoura University, Mansoura, Egypt

### Manuscript Info

#### Manuscript History:

Received: 11 October 2014  
Final Accepted: 15 November 2014  
Published Online: December 2014

#### Key words:

#### \*Corresponding Author

Mohamed M. Eldefrawy

### Abstract

Mesoporous aluminosilicates, have been prepared with various mole ratios of Si/Al and Cethyltrimethylammonium bromide (CTAB). They have been characterized by infrared, small angle XRD and scanning electron microscopy. The results show that incorporation of aluminum ions in the framework of the mesoporous MCM-41 has turned it into an effective cation exchanger. The uptake% values of mercury ions have been increased. The prepared adsorbents were applied for the removal of  $Hg(II)$  from aqueous solution under different experimental conditions by changing contact time, initial concentration of  $Hg(II)$ , pH, presence of interfering ions and solution temperature. Optimum conditions obtained were pH=5 and contact time of 30 min. The experimental data fitted very well with the Pseudo-second-order kinetic model. The calculated thermodynamic parameters ( $\Delta H$ ,  $\Delta S$  and  $\Delta G$ ) detected that the adsorption of  $Hg^{+2}$  onto MCM-41, Al10MCM-41 and Al20MCM-41 is an endothermic and spontaneous process. For experimental data the Langmuir isotherm showed a better fit and maximum adsorption capacity was obtained 100.5, 73.64, 33.92  $mg\ g^{-1}$  for Al10MCM-41, Al20MCM-41 and MCM-41 respectively for an initial concentration range 5–200  $mg\ L^{-1}$ .

Copy Right, IJAR, 2014., All rights reserved

### Introduction

The existence of heavy metals in aqueous systems leads to water toxicity and represents a growing danger for the environment, human beings and other living organisms[1, 2]. In addition to rock leaching due to some external effects [3], these effluents discharge from different anthropogenic sources such as power plants, chemical manufacturing, painting, mining, metallurgy, electroplating and many other industries[4-6]. Mercury, which is not biodegradable, has been classified as a high pollutant by the United States Environmental Protection Agency (EPA) [7] with a maximum contaminant level of 2 ppb in drinking water. When mercury enters water, some biological processes transform it into methylmercury, which is highly toxic and accumulates in fish, in animals that eat fish, and in predators that eat fish-eating animals[8]. Depending on the level of exposure, the impact of mercury exposure can include alteration of the endocrine system, reduced fertility, slower growth and development, and abnormal behavior that affects survival [9, 10]. So, the removal of these toxic metals from aqueous systems is a critical issue from the environment and health point of view. A variety of treatment processes have been applied for mercury removal from aqueous solutions to fulfil permitted limits, including as reduction[11], chemical precipitation [12], membrane separation [13], ion-exchange [14], solvent extraction [15], coagulation [16], and adsorption [17-19]. Among these treatment methods, the mercury adsorption process at the solid-liquid interface was found to be a promising and powerful practice with various advantages:(i) its high efficiency and easiness [20], (ii) its low cost [21] and (iii) the availability of a wide range of adsorbents such as fly ash [22], activated carbon [23], carbon aerogel [24], clay [25], silica surface [26], mesoporous SBA-15 [27], microporous titanosilicate [28] and aluminosilicates [29], polyacrylamide grafted resins [30] and many other adsorbents[31].

Many efforts have been carried out to reduce contaminants from aqueous solutions by adsorption processes because they are simple to operate and cost effective and have also efficient removal capacity. There has been an increasing need for adsorption technology that to have low overall cost, high stability, and to be more effective than the current technology. Nanotechnology offers promising potential for removing mercury from contaminated water and wastewater rapidly, efficiently, and at lower costs. The two major sections of this technology consist of nanoparticles and nanoporous adsorbents. The M41S family of silicate mesoporous molecular sieves with especially large uniform pore structures was synthesized by researchers at Mobil Corporation in 1992. Through this synthesis process, the negatively charged silica species interact with surfactant cations forming a self-assembled mesostructured composite, which after surfactant removal by calcinations an ordered mesoporous material is acquired (Fig. 1). This discovery has led to a scientific revolution in this field. The hexagonal mesophase, named as MCM-41, has highly regular arrays of uniform-sized channels whose diameters are in the range of 15–100 Å. Type of template, the addition of auxiliary organic compounds, and the reaction parameters have an impact on the characteristics of this porous materials [32, 33].

Some features such as (1) easy accessibility to binding sites owing to open framework and regular structure [35, 36], (2) high Hg(II) adsorption capacity due to large surface area and Functionalization capability [37, 38], (3) high selectivity toward Hg(II) adsorption [39], (4) fast adsorption rate due to sufficiently large mesopores [36, 37] have caused MCM-41 to be widely applied by researchers for mercury(II) adsorption studies [40]. For example, MCM-41 was used to remove nitrobenzene, phenol, o-chlorophenol and divalent metal cations from wastewater [41, 42]. MCM-41 was also used to remove volatile organic compounds (VOCs) from indoor air [43-45]. For increase the Hg(II) adsorption efficiency of MCM-41, it should be modified either by organic groups or metal salts [33]. The modification of the mesoporous materials by sevarious functional groups received much attention in adsorption and separation science [46-48]. Modified mesoporous silicas were confirmed to be good adsorbents for the removal of heavy metals from solutions [49-53]. Modified MCM-41 materials were applied to adsorb anionic dyes, mercury [54, 55]. The modification of MCM-41 by organic modifier is an expensive method, but modification by inorganic metal ions is simple, speedy and low cost method.

In this paper, the adsorption studies of mercury on MCM-41 and modified mesoporous aluminosilicate (with Si/Al mole ratio of 10 and 20) were reported. The efficiency of mercury adsorption on the studied adsorbents was studied regarding the pH of mercury solution, initial mercury concentration, and the reaction temperature. In addition, the mechanisms of mercury adsorption were discussed according to the isotherms, kinetics and thermodynamics models.

## 2. Experimental

### 2.1. Reagents

All the chemicals used were of analytical grade from E. Merck (Germany), except cetyltrimethylammonium bromide (CTAB) which was supplied by Aldrich (U.K.).

### 2.2. Apparatus

Organic functional groups present on the adsorbents surface before and after calcination were qualitatively measured using infrared spectroscopy. Sample discs were prepared by mixing 1 mg of the samples with 500 mg of KBr (Merck) in an agate mortar and scanned in a range from 4,000 to 400  $\text{cm}^{-1}$  using a Jasco instrument (Model 6100, Japan). Small-angle XRD spectra were recorded on a Bruker AXS D8 ADVANCE from 2 $\theta$  4 to 10 $^\circ$  using  $\text{CuK}\alpha$  source ( $\lambda = 1.54 \text{ \AA}$ ). Nitrogen adsorption studies were made with a (QUANTACHROME - NOVA 2000 Series) instrument. Nitrogen adsorption and desorption isotherm of the adsorbent was determined at -196  $^\circ\text{C}$  and specific surface area was determined by applying the BET equation to the isotherm. The pore size distribution was calculated using the adsorption branch of the isotherm and the Barrett-Joyner- Halenda (BJH) formula. pH measurements were made with a pH meter (Hi 931401, HANNA and Portugal). Quantitative determination of inorganic ions was made using an inductively coupled plasma-optical emission spectrometer (ICP-OES) of Perkin Elmer/Optima 7000D was employed for the determination of target elements by atomic emission spectrometry. The scanning electron microscope (SEM) images were performed using SEM model Quanta 250 FEG (Field Emission Gun) with accelerating voltage 30 K.V., magnification 14x up to 1000000. A SHIMADZU atomic absorption spectrophotometer AA-6800.

### 2.3. Preparation of MCM-41 and mesoporous aluminosilicates

For preparation of mesoporous aluminosilicate, 12 g CTAB was dissolved in 460 ml of demineralized water, the mixture was stirred for 15 min. after that 80.377 g of sodium silicate nonahydrate was added to the

mixture and it was stirred for 30 min. Then for preparing two materials with different ratios of Si/Al, 1000 ml solutions of  $\text{AlCl}_3$  with concentrations of 0.028 M and 0.014 M were added dropwise to obtain particular materials with mole ratios 10 and 20 respectively. The stirring was sustained for 4 h. Bulky white gelatinous precipitate was formed. The resulting gel was transferred to a plastic vessel and was left for 24 h at room temperature. Then the product was filtered, washed thoroughly with demineralized water then dried at  $50^\circ\text{C}$  for 6 h. For preconditioning of MCM-41 and aluminosilicate; 9 g of each sample was placed in a round bottled flask and 250 ml of  $0.1 \text{ mol l}^{-1}$   $\text{HNO}_3$  was introduced and the mixtures are mechanically stirred at  $80^\circ\text{C}$  for 24 h. These three mixtures were filtered, washed with deionized water then dried at  $80^\circ\text{C}$  overnight. The samples prepared was labeled as follow:  $\text{Al}_x\text{MCM-41}$  where x indicated the Si/Al molar ratio and MCM-41 indicated hexagonal ordered mesoporous silicate[56].

Composition:

30mg (dry mass) amount of sorbent samples was dissolved in 30ml 1M. NaOH. The amounts of aluminum and silicon are determined by ICP technique.

#### 2.4. Procedure for adsorption studies

Adsorption studies of the mercury on the MCM-41,  $\text{Al}_{10}\text{MCM-41}$  and  $\text{Al}_{20}\text{MCM-41}$  adsorbents were carried out using batch method. In this procedure, 20 mg of the studied adsorbents were added to 25 mL of  $10 \text{ mg L}^{-1}$  mercury ions. The pH of the solutions was adjusted with NaOH (0.1M.) and  $\text{HNO}_3$  (0.1M.). The suspension was stirred for preselected period of time using a water shaker bath. Then it was filtered and the amount of mercury ions was investigated by AAS. The percentage of mercury ions that was adsorbed on the adsorbent (% uptake) was figured out by comparing its concentrations before and after adsorption  $C_i$  ( $\text{mg L}^{-1}$ ) and  $C_f$  ( $\text{mg L}^{-1}$ ) respectively.

$$\% \text{ uptake} = \frac{C_i - C_f}{C_i} \times 100 \quad (1)$$

The equilibrium adsorption ( $q_e$ ,  $\text{mmol g}^{-1}$ ) was also determined by following equation:

$$q_e = (C_i - C_f) \times \frac{V}{m} \quad (2)$$

Where V is the volume of the initial solution and m is the mass of the adsorbent.

The effect of solution pH on the adsorption behavior was investigated at room temperature. In batch experiments, 20 mg of MCM-41,  $\text{Al}_{10}\text{MCM-41}$  and  $\text{Al}_{20}\text{MCM-41}$  adsorbents were equilibrated with 25 mL solution containing  $10 \text{ mg L}^{-1}$  of mercury ions at various pHs for 30 min.

In the kinetics study, 20 mg of the studied adsorbents was added to 25 mL glass flasks containing 10 ppm mercury ions solutions. The suspensions were shaken at 150 rpm at room temperature and samples were taken from the solution by fast filtration at different time intervals (2-90 min.).

The effect of adsorbent dose on mercury ions removal was studied by shaking 25 ml of (10 ppm) mercury ions solutions containing different doses of adsorbents (0.01 g–0.15 g) for a period of 30 min. at room temperature.

The isotherm study was performed using various concentrations of metals solutions (5 - 200 ppm). A mixture of 20 mg of the adsorbent materials with 25 mL adsorbate solutions of various initial concentrations was shaken at 150 rpm for 30 min. at  $30^\circ\text{C}$ .

The influence of the temperature on uptake of mercury ions by adsorbent material was studied by equilibrating 20 mg of samples with 25 ml aqueous solution containing different concentration of mercury (II) (5-200 ppm) for 30 min. at different temperatures ranging from 303 K to 328 K.

The effect of foreign ions on the uptake % of  $\text{Hg}^{+2}$  by the studied adsorbents was examined by equilibrating 20 mg adsorbent with 20 ml of 10 ppm for  $\text{Hg}^{+2}$  ions solution containing 100 ppm of various cations and anions.

The applicability for uptake of mercury ions as example of pollutants from different samples of water was investigated for concentration of 10 ppm. The sportive experiments were carried out using 25 ml of clear, filtered, uncontaminated sample solutions after adjusting their pH values to 7.0 and then add 20 mg of sorbent then shaking the mixture for 30 min. The uptake percentage of mercury ions from aqueous solution is computed as presented in (1).

### 3. Results and discussion

#### 3.1. Characterization of adsorbent

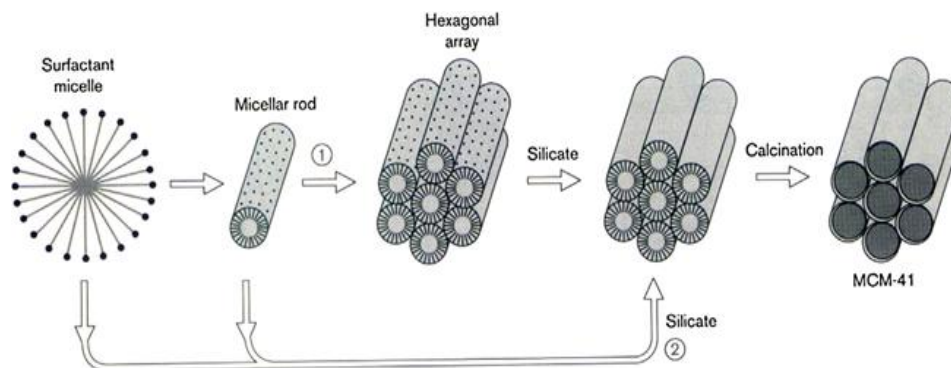
ICP analysis presents the composition of the 3 adsorbents which is (2.1% Al, 21.9% Si) in  $\text{Al}_{10}\text{MCM-41}$  and (0.94% Al, 21.2% Si) in  $\text{Al}_{20}\text{MCM-41}$  samples, while MCM-41 has 27.3% Si in its composition. The results are given in (Table 1).

**Table 1.** Synthesis and surface area data of the adsorbents.

Sample	Si/Al ratio		BET surface area(m <sup>2</sup> /g)	Pore volume(cc/g)	Average pore diameter (Å)
	Added	Found			
Al10MCM-41	10	10.43	875.945	0.415	20.287
Al20MCM-41	20	22.55	953.927	0.467	20.215
MCM-41	-	-	1047.039	0.499	20.174

The small-angle XRD patterns of the as-synthesized and calcined MCM-41, Al10MCM-41 and Al20MCM-41 are presented in Fig. 2. The small angle XRD patterns of samples display a strong diffraction at  $2\theta$  smaller than  $3^\circ$  which approves the formation of mesoporous MCM-41. This result is specialized for hexagonal pore structure. The slight increase in d-spacing and unit cell parameters of Al-MCM-41 compared to its pure silica analog (Table 2) submits the existence of aluminum in the framework. The increase in unit cell parameter on Al incorporation is probably owing to the replacement of shorter Si-O bonds by longer Al-O bonds in the structure. It is important to notice the shift of the reflection maximum in the patterns of the as-synthesized and calcined samples. For example, the as-synthesized Al10MCM-41 has a spacing of 38.65 Å, which over calcinations decreased to 36.18 Å. This decreasing in the d spacing value is owing to contraction of the pore structure, which occurs through the process of calcinations[57].

Table 1 also presents the specific surface area, pore volume and pore size of the samples. The existence of aluminum atoms in MCM-41 type network led to a decrease of specific surface area and total pore volume values[58].

**Fig. 1.** Synthesis scheme for MCM-41 materials [34]

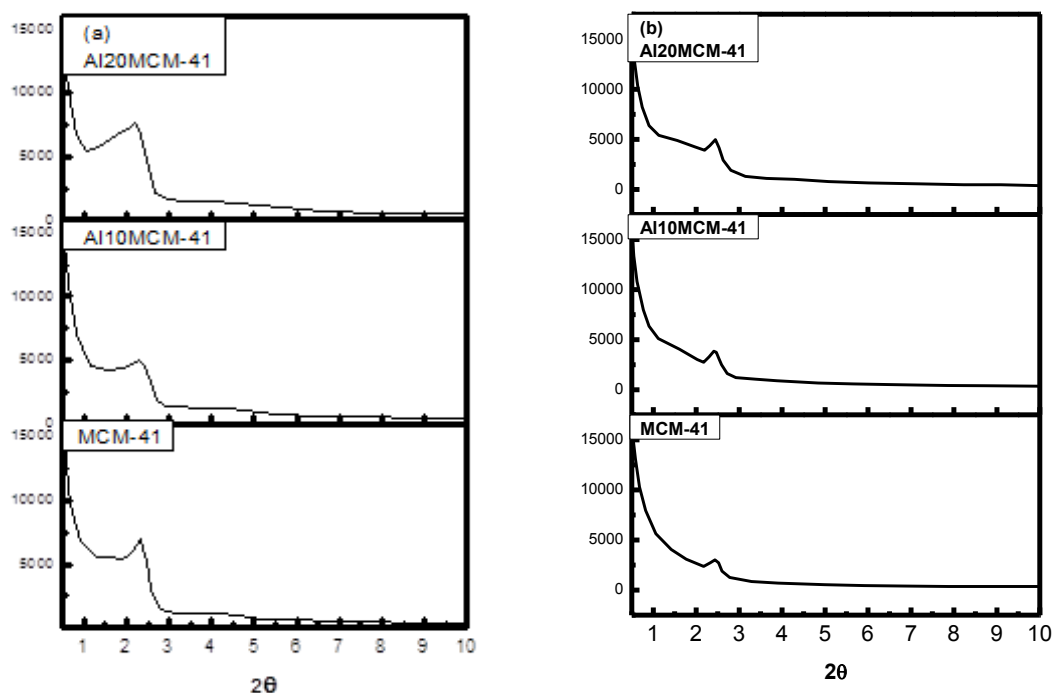


Fig. 2. Small angle XRD patterns of (a) as-synthesized and (b) calcined adsorbents.

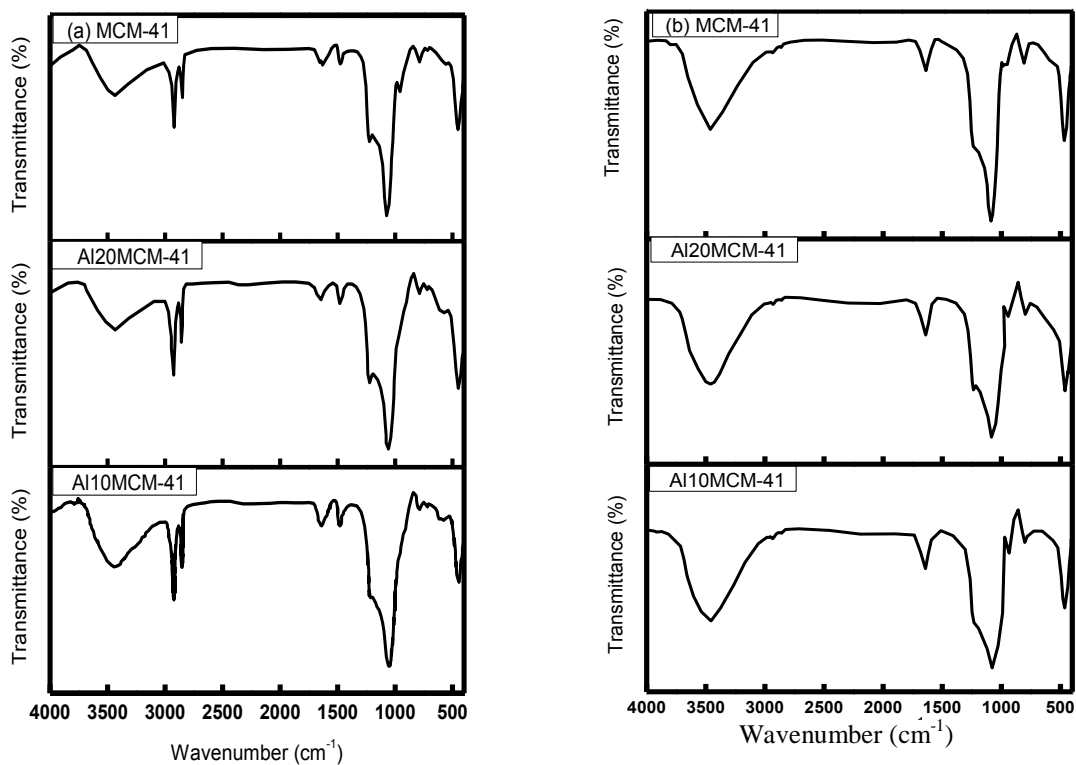
Table 2. Physical characteristics of the adsorbents.

Sample	XRD $d_{100}$ (Å)	Unit cell parameter <sup>a</sup> ( $a_0$ ) (Å)	Position of $2\theta$ (Å)
Uncalcined Al10MCM-41	38.64747	44.63	2.286
Calcined Al10MCM-41	36.18491	41.78	2.4416
Uncalcined Al20MCM-41	40.05598	46.253	2.2056
Calcined Al20MCM-41	36.30816	41.925	2.4333
Uncalcined MCM-41	38.35288	44.286	2.3036
Calcined MCM-41	36.12238	41.7105	2.4458

a. Calculated from the equation  $a_0 = 2d_{100}/\sqrt{3}$ .

IR study of the synthesized adsorbents allowed us to identify characteristic bands of the mesoporous framework of MCM-41 and Al-MCM-41 before and after removing of the template. The infrared spectra of the as-synthesized and calcined samples in the region of 400-4000  $\text{cm}^{-1}$  is displayed in Fig. 3. As can be seen, the as-synthesized sample exhibits absorption bands around (2922, 2852, 1481  $\text{cm}^{-1}$ ) in both MCM-41 and Al10MCM-41 and bands around (2924, 2853, 1479  $\text{cm}^{-1}$ ) in Al20MCM-41 which corresponds to asymmetric and symmetric C-H stretching and C-H bending vibrations of the surfactant molecules. These bands disappear for the calcined sample indicating the total removal of organic material during calcination. Furthermore, absorption bands at 1630, 1640 and 1646  $\text{cm}^{-1}$  in as-synthesized MCM-41, Al10MCM-41 and Al20MCM-41 respectively and also absorption bands at 1631, 1640 and 1638  $\text{cm}^{-1}$  in calcined MCM-41, Al10MCM-41 and Al20MCM-41 respectively, are caused by deformational vibrations of adsorbed water molecules. The absorption bands at 1072, 1054 and 1057  $\text{cm}^{-1}$  in as-synthesized MCM-41, Al10MCM-41 and Al20MCM-41 respectively are due to internal and external asymmetric Si-O stretching

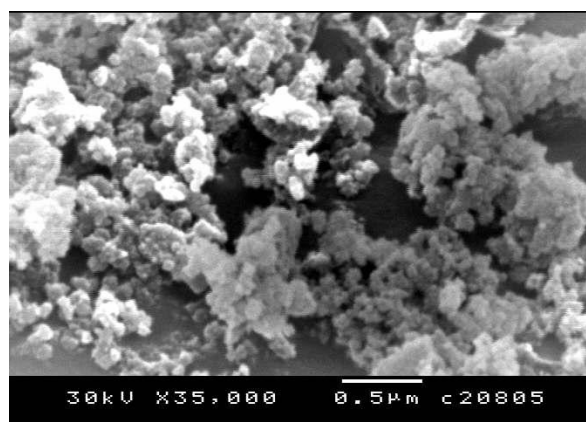
modes. They are shifted to higher frequencies 1090, 1076 and 1080  $\text{cm}^{-1}$  respectively in calcined MCM-41, Al10MCM-41 and Al20MCM-41 respectively. The bands at (794, 458  $\text{cm}^{-1}$ ), (786, 444  $\text{cm}^{-1}$ ) and (788, 449  $\text{cm}^{-1}$ ) are assigned to symmetric Si-O stretching and tetrahedral Si-O bending modes in MCM-41, Al10MCM-41 and Al20MCM-41 respectively and also are slightly shifted to higher frequencies under calcination. Such positive shifts in frequencies would reflect the formation of new Si-O-Si and Si-O-Al bridges during calcination due to an increased network cross-linking and would be accounting for the lattice contraction and structural stabilization that Al-MCM-41 undergoes during calcination. Many authors have taken FT-IR bands appearing around 960  $\text{cm}^{-1}$  in silica-based matrices containing transition metal species as evidence for the isomorphous substitution of Si atoms by heteroatoms because the band was absent in pure silicates[59]. Appearance of a large band near 3420-3454  $\text{cm}^{-1}$  is owing to O-H stretching of surface hydroxyl groups, bridged hydroxyl groups and adsorbed water molecules[60].



**Fig. 3.** IR spectrum of (a) as-synthesized and of (b) calcined adsorbents.

The morphology of the samples was studied by scanning electron microscopy (SEM) Fig. 4. SEM images present the agglomerated nanoparticles with the size range less than 100 nm[61, 62].

(a)



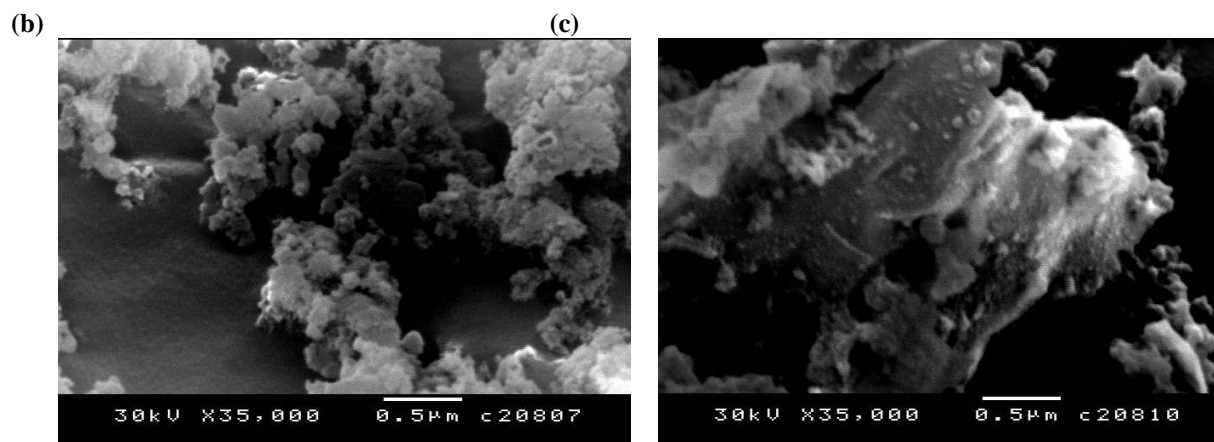


Fig. 4. SEM image of (a) MCM-41, (b) Al10MCM-41 and (c) Al20MCM-41.

### 3.2. Adsorption studies

The pH of a solution is a significant parameter affecting adsorption of metal ions on adsorbents. It is because it not only affects metal species in solution, but also impacts the surface properties of adsorbents in terms of dissociation of functional groups and surface charge. Solutions were prepared at different pH values ranging from 2.0 to 9.0 in order to determine the effect of pH on uptake% of mercury ions on the sorbents. The dependence of pH on the sorption of mercury at an initial concentration of 10 mg/L onto the sorbents is illustrated in Fig. 5. It is evident that the uptake% of mercury are affected by the pH ranging from 2.0 to 9.0. As shown in Fig. 5, the solution pH had an important effect on adsorption, and uptake% were seen to increase with increased solution pH. The optimum pH value appeared to be about 5-6 for mercury removal. At lower pH (<5.0),  $\text{Hg}(\text{II})$  was in the free ionic form of  $\text{Hg}^{2+}$ , and the positively charged hydrogen ions may have competed with the  $\text{Hg}^{2+}$  for binding sites on the surface of the sorbent[63]. Once the surface of sorbent was protonated, the electrostatic interaction decreased. It was not beneficial for  $\text{Hg}^{2+}$  reaction with the surface of the sorbent, resulting in lower uptake% at lower pH. In addition, the typical siliceous hexagonal structure of MCM-41 is destroyed above pH 8, which reduces the amount of mercury sorption [64].The next experiments in this study were proceeded at pH=5[29].

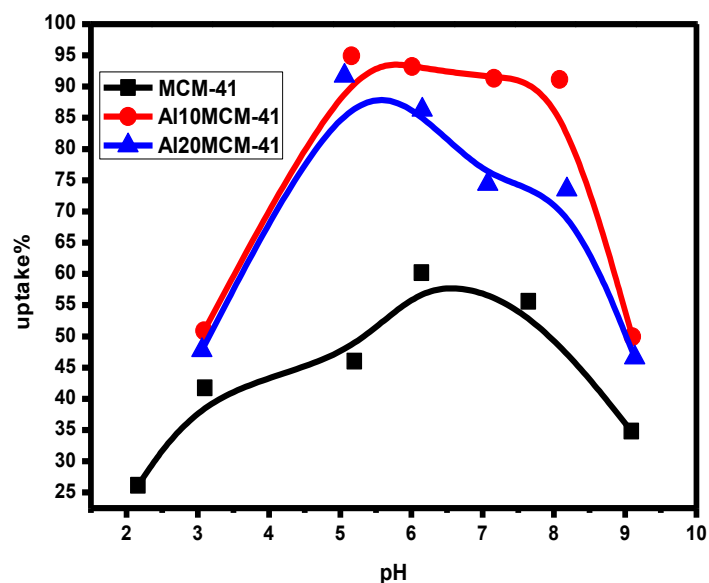


Fig. 5. Effect of pH on uptake percentage of  $\text{Hg}^{2+}$  onto MCM-41, Al10MCM41 and Al20MCM-41.

Kinetic study: The adsorption experiments were proceeded at initial mercury concentration of 10 mg/L at pH=5. The adsorption kinetic second order kinetic results are shown in Fig. 6. It is noticed that the adsorption equilibrium is attained fast in about 30 min. The fast adsorption rate suggests that the silanol groups are readily available and easily attainable probably because the uniform nanoporous channels of the adsorbents facilitate the mercury ions transportation in the process. In order to clarify the adsorption kinetics of mercury onto our studied sorbents, Lagergren's pseudo-first-order and pseudo-second-order kinetic models were applied to the experimental data. The linearized form of the pseudo-first-order rate equation by Lagergren is given as:

$$\ln (q_e - q_t) = \ln q_e - K_1 t \quad (3)$$

Where  $q_t$  and  $q_e$  (mg/g) are the amount of metal ions adsorbed at  $t$  (min.) and equilibrium respectively, and  $K_1$  is the rate constant of the equation ( $\text{min}^{-1}$ ). The adsorption rate constant ( $K_1$ ) can be investigated by plotting of  $\ln (q_e - q_t)$  versus  $t$ . The plots of  $\ln (q_e - q_t)$  versus  $t$  for the Lagergren-first-order model does not fit a pseudo-first-order kinetic model and the  $R^2$  values for this model are extremely low 0.62134, 0.65011 and 0.8095 for MCM-41, Al10MCM-41 and Al20MCM-41, respectively, for the mercury adsorption by these adsorbents. Experimental data were applied also to the pseudo-second-order kinetic model which is given in the following form:

$$t/q = 1/(K_2 q_e^2) + (1/q_e)t \quad (4)$$

Where  $K_2$  ( $\text{g}/\text{mg}\cdot\text{min}$ ) is the rate constant of the second-order equation,  $q_e$  is the amount of adsorption equilibrium (mg/g) and  $q_t$  (mg/g) the amount of adsorption at time  $t$  (min). The linear plots of  $t/q_e$  versus  $t$  for pseudo-second-order model for the adsorption of  $\text{Hg}^{+2}$  onto MCM-41, Al10MCM-41 and Al20MCM-41 are shown in Fig. 6. The rate constants ( $K_2$ ), correlation coefficient of the plots together with the  $q_e$  value is given in Table 3. These results pointed out that the adsorption of mercury ions onto the studied sorbents follows very well the pseudo-second-order kinetics[40, 65].

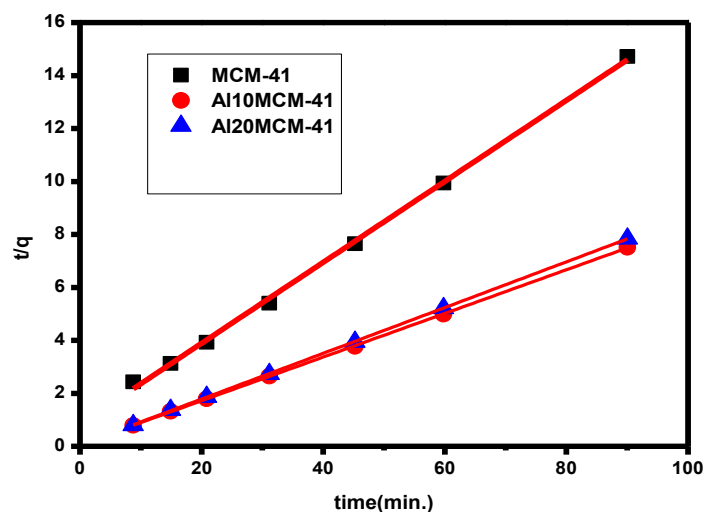


**Fig. 6.** Pseudo-second-order adsorption kinetic of  $\text{Hg}^{+2}$  onto MCM-41, Al10MCM41 and Al20MCM-41 sorbents.

**Table 3:** Parameters for adsorption of  $\text{Hg}^{+2}$  onto MCM-41, Al10MCM-41 and Al20MCM-41 derived from the pseudo-first and pseudo-second-order models.

Sample	Pseudo-first-order			Pseudo-second-order		
	$q_e$ (mg/g)	$-K_1$ ( $\text{min}^{-1}$ )	$R^2$	$K_2$ ( $\text{g}/\text{mg}\cdot\text{min}$ )	$q_e$ (mg/g)	$R^2$
Al10MCM-41	6.79	0.1406	0.88	0.10	12.2	0.9999
Al20MCM-41	3.55	0.1149	0.80	0.13	11.7	0.9999

<b>MCM-41</b>	<b>4.13</b>	<b>0.0680</b>	<b>0.96</b>	<b>0.03</b>	<b>6.5</b>	<b>0.999</b>
---------------	-------------	---------------	-------------	-------------	------------	--------------

Effect of adsorbent dosage: The results of the experiments with changing adsorbent dose are displayed in Fig. 7. Increasing in the adsorbent dose from 0.02 g to 0.15 g/25 ml increased the uptake % of  $\text{Hg}^{+2}$  ions. This is due to the fact that as the adsorbent dosage is increased, more adsorption sites are available for sorbate which cause enhancing in the percent of mercury (II) uptake.

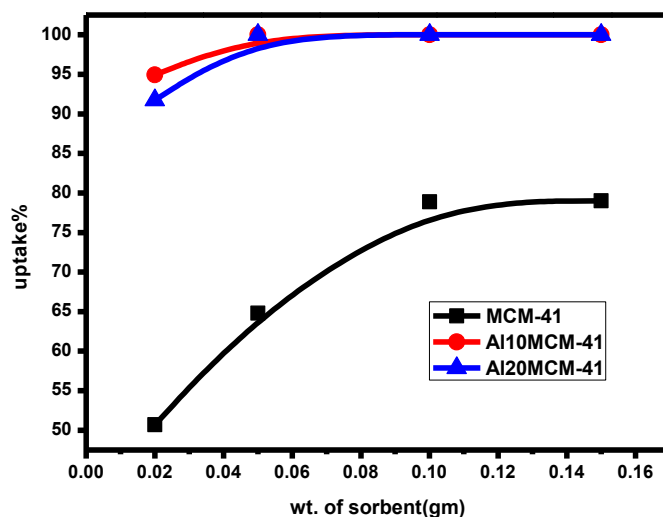


**Fig. 7.** Effect of MCM-41, Al10MCM-41 and Al20MCM-41 concentration on the uptake percentage of  $\text{Hg}^{+2}$  ions.

Effect of initial concentration: For isotherm study, the effect of initial concentration on the removal efficiency of  $\text{Hg}^{2+}$  was studied in the concentration range of 5–200  $\text{mg L}^{-1}$  for Al10MCM-41, Al20MCM-41 and MCM-41 Fig. 8. When initial concentrations increased, the adsorption rate increased and removal efficiency decreased. Because of the increasing number of  $\text{Hg}^{2+}$  cations in more concentrated solutions, effective interactions between metal ions and adsorption sites increased [66].

The actual amount of  $\text{Hg}^{2+}$  adsorbed per unit mass of the studied adsorbents increased with increase in  $\text{Hg}^{+2}$  concentration. It means that the adsorption is highly dependent on initial concentration of  $\text{Hg}^{+2}$ . This is due to the fact that at lower concentration, the ratio of the initial number of mercury ions to the available surface area is low subsequently the fractional adsorption becomes independent of initial concentration. However, at high concentration the available sites of adsorption becomes fewer and hence the uptake percentage of  $\text{Hg}^{+2}$  is dependent upon initial concentration.

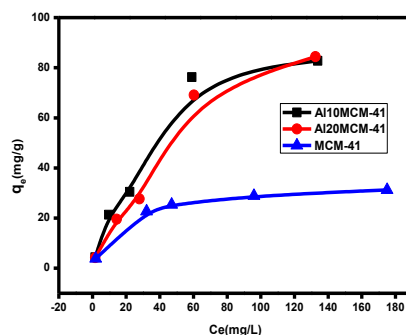


**Fig. 8.** Effect of initial concentration on adsorption of  $\text{Hg}^{+2}$  on MCM-41, Al10MCM-41 and Al20MCM-41 at 30°C.

Adsorption isotherm: The adsorption isotherms of  $\text{Hg}(\text{II})$  onto mesoporous sorbents were explained according to two parameter models, Langmuir and Freundlich models. Freundlich and Langmuir models are the

most common isotherms for determining adsorption phenomena. Equilibrium data for mercury adsorption on molecular sieve were applied to Freundlich and Langmuir equations. The adsorption isotherm is plotted in Figs. 9&10. The Langmuir model assumes that uptake of metal ions occur on a homogeneous surface by monolayer adsorption without interaction between adsorbed ions. The model is described in the following equation form:

$$\frac{1}{q_e} = \frac{1}{bq_m} + \frac{1}{C_e} \quad (5)$$

Where  $b$  is Langmuir equilibrium constant (l/mg), and  $q_m$  (mg/g) is the monolayer adsorption capacity. Both are determined from a plot  $C_e/q_e$  versus  $C_e$ . As seen in Fig. 9, it is observed that the adsorption data fit the Langmuir equation very well and the equation constant values  $q_m$  and  $b$ , calculated from the experimental data (Table 4). Langmuir equation is the most common model employed to characterize the adsorption process in homogenous systems. For comparative purposes the experimental data have been fitted to the well-known Freundlich equation; Freundlich model suggests that uptake or adsorption of metal ions occurs on the heterogeneous surface by monolayer adsorption.

The equation of this model is described following like this:

$$\log q_e = \log K_F + 1/n \log C_e \quad (6)$$

Where  $K_F$  and  $1/n$  are Freundlich constants related to adsorption capacity and adsorption intensity, respectively. These parameters are determined from a plot  $\log q$  versus  $\log C_e$  (Fig. 10). From the values of  $R^2$  summarized in (Table 4) it is clear that Langmuir equation provides a better fitting than Freundlich [65].

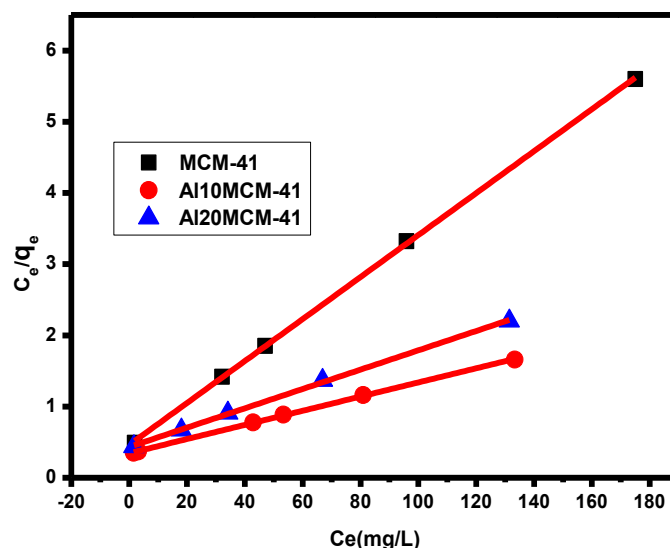


Fig. 9. Langmuir adsorption isotherm for  $Hg^{+2}$  on MCM-41, Al10MCM-41 and Al20MCM-41 at 30°C.

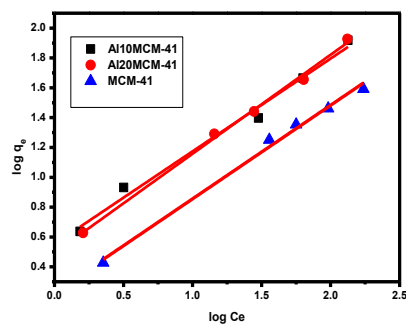


Fig. 10. Freundlich adsorption isotherm for  $Hg^{+2}$  on MCM-41, Al10MCM-41 and Al20MCM-41 sorbents at 30°C.

Table 4: Fitting parameters of adsorption model isotherms.

Sample	Langmuir fitting parameters			Freundlich fitting parameters		
	R <sup>2</sup>	b	q <sub>m</sub>	R <sup>2</sup>	K <sub>f</sub>	1/n
MCM-41	0.999	0.064	33.921	0.992	1.6907	0.628
Al10MCM-41	0.999	0.029	100.50	0.984	3.573	0.621
Al20MCM-41	0.999	0.031	73.64	0.996	3.119	0.664

By comparing the several low-cost adsorbents and some mesoporous materials with our synthesized MCM-41, Al10MCM-41, Al20MCM-41 it can be said that they have high sorption capacity for Hg(II). From these results, it can be concluded that our studied sorbents are expected to be a good material for removal of Hg(II) in polluted water.

**Table 5:** Sorption capacity for mercury ions of different common low-cost sorbents

Sorbent	Sorption Capacity (mg/g)	Reference
Hybrid mesoporous aluminosilicate	20.655	[64]
4-aminoantipyrine immobilized bentonite	52.9	[67]
Polyacrylamide aerogel	13.75	[31]
Silica aerogel	9.17	[31]
Hybrid aerogel	13.69	[31]
Mesoporous MCM-41	33.921	This study
Mesoporous Al10MCM-41	100.5	This study
Mesoporous Al20MCM-41	73.64	This study

Effect of temperature: A thermodynamic study was conducted at different temperature (30, 45 and 55 °C). The data was plotted in Van't Hoff plot as  $\ln K_d$  vs.  $1/T$  which give straight line (Fig. 11). The change in standard free energy of adsorption ( $\Delta G^\circ$ ) was calculated from the following equation:

$$\Delta G^\circ = -RT \ln K_d \quad (7)$$

$$\text{Where, } K_d = \frac{q_e}{C_e} \times 1000 \quad (8)$$

Where,  $K_d$  is the equilibrium constant at temperature  $T$  in K [68] and  $R$  which is gas constant (8.314 J/mol K). Indication of  $q_e$  and  $C_e$  are the equilibrium concentration of  $\text{Hg}^{+2}$  on the studied adsorbents (mg/g) and in solution (mg/L), respectively.

Values of enthalpy and entropy ( $\Delta H^\circ$  and  $\Delta S^\circ$ ) were calculated from the slope and intercept of the plot. The data represented in Table 6 indicate that: The negative values of  $\Delta G^\circ$  are signs of spontaneity of the sorption and increase in the numerical value of  $\Delta G^\circ$  with increase in temperature indicates temperature favorable sorption phenomena. The positive value of enthalpy change ( $\Delta H^\circ$ ) confirms that the sorption process is endothermic. The positive value of entropy ( $\Delta S^\circ$ ) submits the increase in randomness at the solid-solution interface by the fixation of mercury ions on the sorbents. Mercury ions in aqueous media are hydrated. The ions were sorbed on the sorbents surfaces, water molecules formerly bounded to the mercury ions were released and dispersed in solution, resulting in an increase in entropy. Values of thermodynamic parameters are presented in Table 6. It seemed that the equilibrium adsorption capacity was obviously improved by increasing temperature from 303 K to 328 K. It is due to the fact that the effective adsorption sites on the adsorbent became more and mercury diffusion process may be promoted under higher temperature conditions in which mercury ion moves more quickly solution. In addition to this, water viscosity decreases and adsorption sites on the adsorbent become more energetic as temperature increases [64].

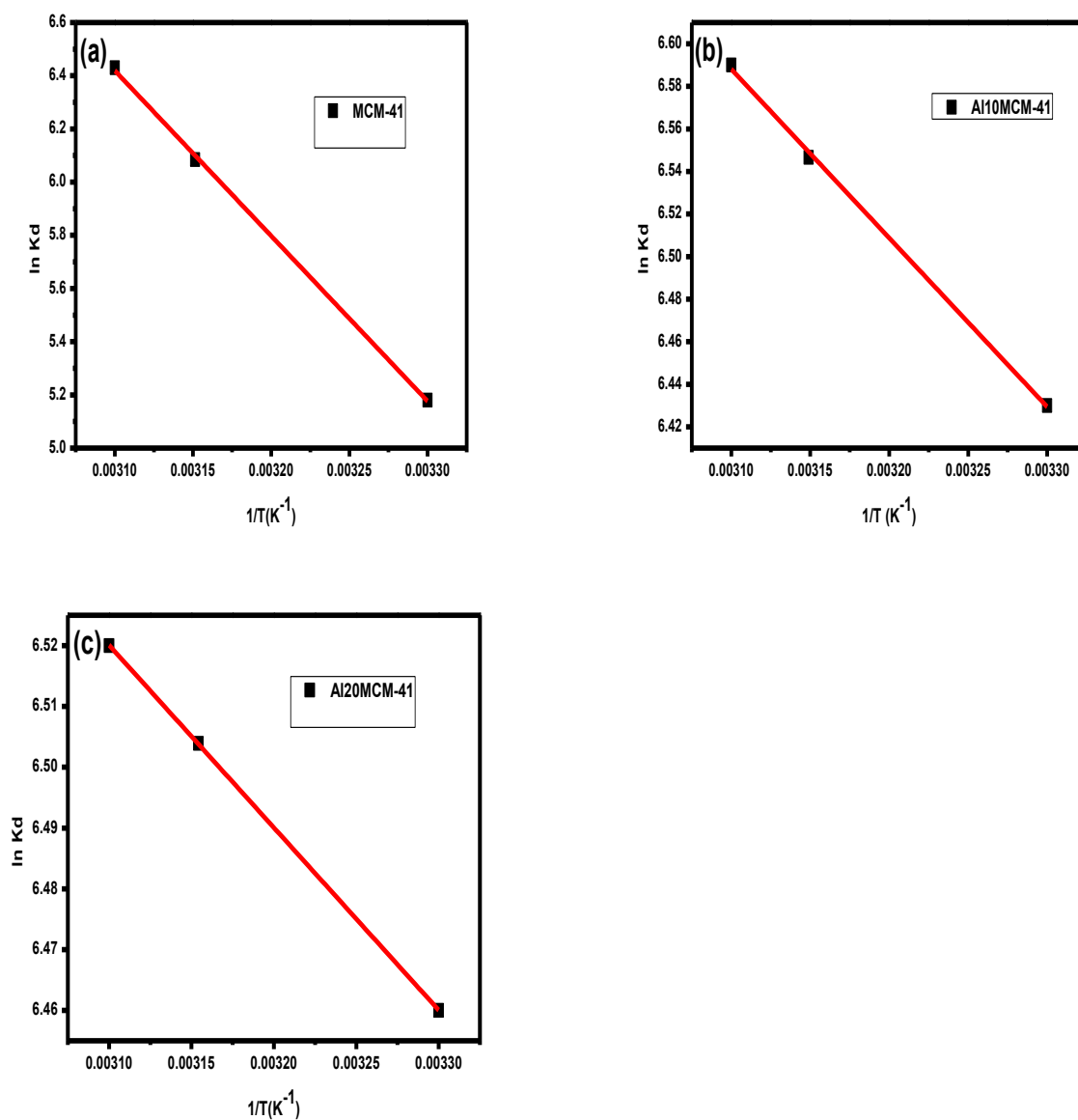


**Fig. 11.** Van't Hoff plot for  $Hg^{+2}$  on (a) MCM-41, (b) Al10MCM-41 and (c) Al20MCM-41.

**Table 6:** Thermodynamic parameters for the sorption of  $Hg^{+2}$  on the prepared sorbents.

Sample	$-\Delta G^{\circ}(\text{J/mol})$	$+\Delta H^{\circ}(\text{J/mol})$	$\Delta S^{\circ}(\text{J/mol.K})$
<b>Al10MCM-41</b>			
303 K	16198.08	6597.5106	75.22257
318 K	17308.45		
328 K	17970.88		

<b>Al20MCM-41</b> <b>303 K</b> <b>318 K</b> <b>328 K</b>	<b>16273.66</b> <b>17195.38</b> <b>17779.99</b>	<b>2496.45719</b>	<b>61.94703</b>
<b>MCM-41</b> <b>303 K</b> <b>318 K</b> <b>328 K</b>	<b>13049.16</b> <b>16088.05</b> <b>17534.56</b>	<b>51667.5808</b>	<b>213.5384</b>

Effect of foreign ions: Natural water matrix (anions and cations) can intensely affect the removal of heavy metals on the surface of sorbents therefore the uptake % of  $\text{Hg}^{+2}$  by Al10MCM-41 and Al20MCM-41 was examined in the presence of some possible matrix ions such as phosphate, chloride, sulphate, nitrite, bicarbonate,  $\text{Na}^+$ ,  $\text{K}^+$ ,  $\text{Mg}^{+2}$  and  $\text{Ca}^{2+}$ . The impact of these foreign ions on the uptake% of mercury ions was studied in the presence of high concentration of them to magnify their effect on the adsorption capacity of mercury ions on the studied sorbents. The results are shown in Table 7.

**Table 7:** Effect of foreign ions on the sorption of  $\text{Hg}^{+2}$ .

Foreign Ion (100 mg/L)	Al10MCM-41 Uptake%	Al20MCM-41 Uptake%
$\text{K}^+$	<b>87.49%</b>	<b>84.25%</b>
$\text{Na}^+$	<b>95.1%</b>	<b>91.75%</b>
$\text{Mg}^{+2}$	<b>90.02%</b>	<b>85.39%</b>
$\text{Ca}^{+2}$	<b>86.69%</b>	<b>82.87%</b>
$\text{NO}_2^-$	<b>95.2%</b>	<b>91.26%</b>
$\text{HCO}_3^-$	<b>95.2%</b>	<b>90.91%</b>
$\text{Cl}^-$	<b>92.66%</b>	<b>88.38%</b>
$\text{SO}_4^{-2}$	<b>95.1%</b>	<b>91.72%</b>
$\text{PO}_4^{-3}$	<b>92.32%</b>	<b>88.15%</b>

Analytical application : As shown in Table 8, the applicability of the MCM-41, Al10MCM-41 and Al20MCM-41 for uptake of  $\text{Hg}^{+2}$  from different samples of natural water was studied for spiked concentration (10 ppm). Samples were filtered using a sintered glass G4. The pH and total dissolved salts (TDS)

were determined then the samples were acidified with concentrated HNO<sub>3</sub> acid to pH approximately equals 2 and preserved in polyethylene vessels. The sportive experiments were carried out using 25 ml of clear, filtered, uncontaminated sample solutions after adjusting their pH values to 7.0 and then add 0.02 g of the sorbent before shaking the mixture.

**Table 8:** Analytical application.

Water sample	MCM-41	Al10MCM-41 % Uptake	Al20MCM-41
Ras El Bar El Gerby <sup>e</sup>	44.56%	93.7%	89.7%
El Mansoura City <sup>a</sup>	46.4%	95.9%	91.9%
Al Dqahlya Dekrnis <sup>b</sup>	45.89%	95.89%	91.5%
Al Dqahlya Gamasa <sup>e</sup>	44.02%	93.2%	89.1%
Ras El Bar Tongue <sup>e</sup>	43.98%	93.1%	89%
Damietta Port Damietta <sup>e</sup>	45.1%	94%	90.1%
El Manzalah Lake <sup>c,d</sup>	45%	92.5%	88.65%
Al Dqahlya Meat Anter <sup>b</sup>	45.71%	95.2%	91.01%

Note: i-All measured RSD ranges from 1-5%.

ii-a=Tap water, b=Nile water, c=Waste water, d=Lake water, e=Sea water.

#### 4. Conclusions

From the results achieved in this work, the following conclusions can be drawn:

- (1) Mesoporous molecular sieves MCM-41, Al10MCM-41, Al20MCM-41 were synthesized with sodium silicate nonahydrate as silica source. The prepared mesoporous sorbents have surface areas of 875.95, 953.93, 1047.04 m<sup>2</sup>/g and average pore volume of 0.42, 0.47, 0.5 cc/g for Al10MCM-41, Al20MCM-41 and MCM-41, respectively.
- (2) Al10MCM-41 and Al20MCM-41 have higher sorption capacity for Hg(II) than MCM-41. The adsorption isotherms of Hg(II) on the prepared mesoporous sorbents can be described well by the Langmuir model. The maximum adsorption of Hg(II) on Al10MCM-41, Al20MCM-41 and MCM-41 is 100.5, 73.64, 33.92 mg/g, respectively.
- (3) The sorption of Hg(II) on Al10MCM-41, Al20MCM-41 and MCM-41 is strongly dependent on pH values.
- (4) The thermodynamic parameters calculated from the temperature dependent sorption isotherms indicate that the sorption process is spontaneous and endothermic.

#### 5. References

1. Nriagu, J.O. and J.M. Pacyna, Quantitative assessment of worldwide contamination of air, water and soils by trace metals. *nature*, 1988. **333**(6169): p. 134-139.
2. Mance, G., International controls, in *Pollution Threat of Heavy Metals in Aquatic Environments*. 1987, Springer. p. 313-330.

3. Da Pelo, S., et al., Release of toxic elements from rocks and mine wastes at the Furtei gold mine (Sardinia, Italy). *Journal of Geochemical Exploration*, 2009. **100**(2): p. 142-152.
4. Dong, J., Z. Xu, and F. Wang, Engineering and characterization of mesoporous silica-coated magnetic particles for mercury removal from industrial effluents. *Applied Surface Science*, 2008. **254**(11): p. 3522-3530.
5. Meena, A.K., et al., Removal of heavy metal ions from aqueous solutions using carbon aerogel as an adsorbent. *Journal of Hazardous Materials*, 2005. **122**(1): p. 161-170.
6. Xie, J., X. Liu, and J. Liang, Absorbency and adsorption of poly (acrylic acid-co-acrylamide) hydrogel. *Journal of applied polymer science*, 2007. **106**(3): p. 1606-1613.
7. Keith, L. and W. Telliard, ES&T special report: priority pollutants: Ia perspective view. *Environmental Science & Technology*, 1979. **13**(4): p. 416-423.
8. Chasar, L.C., et al., Mercury cycling in stream ecosystems. 3. Trophic dynamics and methylmercury bioaccumulation. *Environmental science & technology*, 2009. **43**(8): p. 2733-2739.
9. Tan, S.W., J.C. Meiller, and K.R. Mahaffey, The endocrine effects of mercury in humans and wildlife. *Critical reviews in toxicology*, 2009. **39**(3): p. 228-269.
10. Zhu, X., et al., The endocrine disruptive effects of mercury. *Environmental health and preventive medicine*, 2000. **4**(4): p. 174-183.
11. Oehmen, A., et al., The effect of carbon source on the biological reduction of ionic mercury. *Journal of hazardous materials*, 2009. **165**(1): p. 1040-1048.
12. Matlock, M.M., B.S. Howerton, and D.A. Atwood, Irreversible precipitation of mercury and lead. *Journal of hazardous materials*, 2001. **84**(1): p. 73-82.
13. Barron-Zambrano, J., et al., Mercury removal and recovery from aqueous solutions by coupled complexation-ultrafiltration and electrolysis. *Journal of membrane science*, 2004. **229**(1): p. 179-186.
14. Anirudhan, T., L. Divya, and M. Ramachandran, Mercury (II) removal from aqueous solutions and wastewaters using a novel cation exchanger derived from coconut coir pith and its recovery. *Journal of hazardous materials*, 2008. **157**(2): p. 620-627.
15. Li, Z., et al., A new room temperature ionic liquid 1-butyl-3-trimethylsilylimidazolium hexafluorophosphate as a solvent for extraction and preconcentration of mercury with determination by cold vapor atomic absorption spectrometry. *Talanta*, 2007. **71**(1): p. 68-72.
16. Terashima, Y., H. Ozaki, and M. Sekine, Removal of dissolved heavy metals by chemical coagulation, magnetic seeding and high gradient magnetic filtration. *Water Research*, 1986. **20**(5): p. 537-545.
17. Basha, S., Z. Murthy, and B. Jha, Sorption of Hg (II) onto *Carica papaya*: Experimental studies and design of batch sorber. *Chemical Engineering Journal*, 2009. **147**(2): p. 226-234.
18. Liu, X., et al., Specific mercury (II) adsorption by thymine-based sorbent. *Talanta*, 2009. **78**(1): p. 253-258.
19. Rae, I.B., S.W. Gibb, and S. Lu, Biosorption of Hg from aqueous solutions by crab carapace. *Journal of hazardous materials*, 2009. **164**(2): p. 1601-1604.
20. Manchester, S., et al., High capacity mercury adsorption on freshly ozone-treated carbon surfaces. *Carbon*, 2008. **46**(3): p. 518-524.
21. Wang, S. and H. Wu, Environmental-benign utilisation of fly ash as low-cost adsorbents. *Journal of Hazardous Materials*, 2006. **136**(3): p. 482-501.
22. López-Antón, M.A., et al., The influence of carbon particle type in fly ashes on mercury adsorption. *Fuel*, 2009. **88**(7): p. 1194-1200.
23. Chung, S.T., K.I. Kim, and Y.R. Yun, Adsorption of elemental mercury vapor by impregnated activated carbon from a commercial respirator cartridge. *Powder Technology*, 2009. **192**(1): p. 47-53.
24. Goel, J., et al., Removal of mercury (II) from aqueous solution by adsorption on carbon aerogel: Response surface methodological approach. *Carbon*, 2005. **43**(1): p. 197-200.
25. Guerra, D.L., R.R. Viana, and C. Airoidi, Adsorption of mercury cation on chemically modified clay. *Materials research bulletin*, 2009. **44**(3): p. 485-491.
26. Belyakova, L.A., O.M. Shvets, and D.Y.e. Lyashenko, Formation of the nanostructure on a silica surface as mercury (II) ions adsorption sites. *Inorganica Chimica Acta*, 2009. **362**(7): p. 2222-2230.
27. Aguado, J., J.M. Arsuaga, and A. Arencibia, Influence of synthesis conditions on mercury adsorption capacity of propylthiol functionalized SBA-15 obtained by co-condensation. *Microporous and Mesoporous Materials*, 2008. **109**(1): p. 513-524.
28. Lopes, C., et al., Removal of Hg<sup>2+</sup> ions from aqueous solution by ETS-4 microporous titanosilicate—Kinetic and equilibrium studies. *Chemical Engineering Journal*, 2009. **151**(1): p. 247-254.

29. Wu, X.-W., et al., The synthesis of mesoporous aluminosilicate using microcline for adsorption of mercury (II). *Journal of colloid and interface science*, 2007. **315**(2): p. 555-561.
30. Yavuz, E., B.F. Senkal, and N. Bıcak, Poly (acrylamide) grafts on spherical polyvinyl pyridine resin for removal of mercury from aqueous solutions. *Reactive and Functional Polymers*, 2005. **65**(1): p. 121-125.
31. Ramadan, H., A. Ghanem, and H. El-Rassy, Mercury removal from aqueous solutions using silica, polyacrylamide and hybrid silica-polyacrylamide aerogels. *Chemical Engineering Journal*, 2010. **159**(1): p. 107-115.
32. Dubois, M., T. Gulik-Krzywicki, and B. Cabane, Growth of silica polymers in a lamellar mesophase. *Langmuir*, 1993. **9**(3): p. 673-680.
33. Raji, F. and M. Pakizeh, Study of Hg (II) species removal from aqueous solution using hybrid ZnCl<sub>2</sub>-MCM-41 adsorbent. *Applied Surface Science*, 2013. **282**: p. 415-424.
34. Sever, R.R., et al., Vapor-phase silylation of MCM-41 and Ti-MCM-41. *Microporous and mesoporous materials*, 2003. **66**(1): p. 53-67.
35. Mercier, L. and T.J. Pinnavaia, Access in mesoporous materials: advantages of a uniform pore structure in the design of a heavy metal ion adsorbent for environmental remediation. *Advanced Materials*, 1997. **9**(6): p. 500-503.
36. Walcarius, A., M. Etienne, and B. Lebeau, Rate of access to the binding sites in organically modified silicates. 2. Ordered mesoporous silicas grafted with amine or thiol groups. *Chemistry of materials*, 2003. **15**(11): p. 2161-2173.
37. Walcarius, A. and C. Delacôte, Rate of access to the binding sites in organically modified silicates. 3. Effect of structure and density of functional groups in mesoporous solids obtained by the co-condensation route. *Chemistry of materials*, 2003. **15**(22): p. 4181-4192.
38. Delacôte, C., et al., Factors affecting the reactivity of thiol-functionalized mesoporous silica adsorbents toward mercury (II). *Talanta*, 2009. **79**(3): p. 877-886.
39. Idris, S.A., S.R. Harvey, and L.T. Gibson, Selective extraction of mercury (II) from water samples using mercapto functionalised-MCM-41 and regeneration of the sorbent using microwave digestion. *Journal of hazardous materials*, 2011. **193**: p. 171-176.
40. Raji, F. and M. Pakizeh, Kinetic and thermodynamic studies of Hg (II) adsorption onto MCM-41 modified by ZnCl<sub>2</sub>. *Applied Surface Science*, 2014. **301**: p. 568-575.
41. Mangrulkar, P.A., et al., Adsorption of phenol and *o*-chlorophenol by mesoporous MCM-41. *Journal of hazardous materials*, 2008. **160**(2): p. 414-421.
42. Northcott, K.A., et al., The adsorption of divalent metal cations on mesoporous silicate MCM-41. *Chemical Engineering Journal*, 2010. **157**(1): p. 25-28.
43. Qin, Q., J. Ma, and K. Liu, Adsorption of nitrobenzene from aqueous solution by MCM-41. *Journal of colloid and interface science*, 2007. **315**(1): p. 80-86.
44. Shao, X., et al., Effects of surface acidities of MCM-41 modified with MoO<sub>3</sub> on adsorptive desulfurization of gasoline. *Applied Surface Science*, 2012. **263**: p. 1-7.
45. Cai, C., H. Wang, and J. Han, Synthesis and characterization of ionic liquid-functionalized aluminosilicate MCM-41 hybrid mesoporous materials. *Applied Surface Science*, 2011. **257**(23): p. 9802-9808.
46. Jal, P., S. Patel, and B. Mishra, Chemical modification of silica surface by immobilization of functional groups for extractive concentration of metal ions. *Talanta*, 2004. **62**(5): p. 1005-1028.
47. Li, J., et al., Synthesis and characterization of imidazole-functionalized SBA-15 as an adsorbent of hexavalent chromium. *Materials Letters*, 2007. **61**(14): p. 3197-3200.
48. Fryxell, G.E., et al., Design and synthesis of self-assembled monolayers on mesoporous supports (SAMMS): the importance of ligand posture in functional nanomaterials. *Journal of Materials Chemistry*, 2007. **17**(28): p. 2863-2874.
49. Pérez-Quintanilla, D., et al., 2-Mercaptothiazoline modified mesoporous silica for mercury removal from aqueous media. *Journal of hazardous materials*, 2006. **134**(1): p. 245-256.
50. Perez-Quintanilla, D., et al., Mesoporous silica functionalized with 2-mercaptopyridine: synthesis, characterization and employment for Hg (II) adsorption. *Microporous and mesoporous materials*, 2006. **89**(1): p. 58-68.
51. Pérez-Quintanilla, D., et al., Preparation of 2-mercaptopbenzothiazole-derivatized mesoporous silica and removal of Hg (II) from aqueous solution. *Journal of Environmental Monitoring*, 2006. **8**(1): p. 214-222.
52. Antochshuk, V., et al., Benzoylthiourea-modified mesoporous silica for mercury (II) removal. *Langmuir*, 2003. **19**(7): p. 3031-3034.

53. Lin, K., et al., Ordered mesoporous titanosilicates with better catalytically active titanium sites assembled from preformed titanosilicate precursors with zeolite building units in alkaline media. *Microporous and mesoporous materials*, 2004. **72**(1): p. 193-201.
54. Qin, Q., J. Ma, and K. Liu, Adsorption of anionic dyes on ammonium-functionalized MCM-41. *Journal of hazardous materials*, 2009. **162**(1): p. 133-139.
55. Furtado, A., et al., MCM-41 impregnated with active metal sites: synthesis, characterization, and ammonia adsorption. *Microporous and Mesoporous Materials*, 2011. **142**(2): p. 730-739.
56. Sepehrian, H., et al., Adsorption studies of heavy metal ions on mesoporous aluminosilicate, novel cation exchanger. *Journal of hazardous materials*, 2010. **176**(1): p. 252-256.
57. Suyanta, S., et al., SYNTHESIS AND CHARACTERIZATION OF MESOPOROUS ALUMINOSILICATES Al-MCM-41 AND INVESTIGATION OF ITS THERMAL, HYDROTHERMAL AND ACIDITY STABILITY. *Indonesian Journal of Chemistry*, 2010. **10**(1): p. 41-45.
58. Nastase, S., et al., Ordered mesoporous silica and aluminosilicate-type matrix for amikacin delivery systems. *Microporous and Mesoporous Materials*, 2013. **182**: p. 32-39.
59. Eimer, G.A., et al., Synthesis and characterization of Al-MCM-41 and Al-MCM-48 mesoporous materials. *Catalysis letters*, 2002. **78**(1-4): p. 65-75.
60. Boukoussa, B., et al., Adsorption of yellow dye on calcined or uncalcined Al-MCM-41 mesoporous materials. *Arabian Journal of Chemistry*, 2013.
61. Abdollahi-Alibeik, M. and E. Heidari-Torkabad, H<sub>3</sub>PW<sub>12</sub>O<sub>40</sub>/MCM-41 nanoparticles as efficient and reusable solid acid catalyst for the synthesis of quinoxalines. *Comptes Rendus Chimie*, 2012. **15**(6): p. 517-523.
62. Zhai, S.-R., I. Kim, and C.-S. Ha, Structural and catalytic characterization of nanosized mesoporous aluminosilicates synthesized via a novel two-step route. *Catalysis Today*, 2008. **131**(1): p. 55-60.
63. Zheng, S., et al., Synthesis, characterization and photocatalytic properties of titania-modified mesoporous silicate MCM-41. *J. Mater. Chem.*, 2000. **10**(3): p. 723-727.
64. Liu, M., et al., Synthesis, characterization, and mercury adsorption properties of hybrid mesoporous aluminosilicate sieve prepared with fly ash. *Applied surface science*, 2013. **273**: p. 706-716.
65. Li, G., et al., Effective heavy metal removal from aqueous systems by thiol functionalized magnetic mesoporous silica. *Journal of hazardous materials*, 2011. **192**(1): p. 277-283.
66. Javadian, H. and M. Taghavi, Application of novel Polypyrrole/thiol-functionalized zeolite Beta/MCM-41 type mesoporous silica nanocomposite for adsorption of Hg<sup>2+</sup> from aqueous solution and industrial wastewater: Kinetic, isotherm and thermodynamic studies. *Applied Surface Science*, 2014. **289**: p. 487-494.
67. Wang, Q., et al., Adsorption of chromium (III), mercury (II) and lead (II) ions onto 4-aminoantipyrine immobilized bentonite. *Journal of hazardous materials*, 2011. **186**(2): p. 1076-1081.
68. Yang, Y., et al., Biosorption of Acid Black 172 and Congo Red from aqueous solution by nonviable *Penicillium* YW 01: Kinetic study, equilibrium isotherm and artificial neural network modeling. *Bioresource technology*, 2011. **102**(2): p. 828-834.